PROCEEDINGS, Thirty-Ninth Workshop on Geothermal Reservoir Engineering
Stanford University, Stanford, California, February 24-26, 2014
SGP-TR-202

Hydraulic Response to Thermal Stimulation Efforts at Raft River Based on Stepped Rate Injection Testing

Mitchell Plummer[1], Carl Palmer[1], Rob Podgorney[1], Jacob Bradford[2], Joseph Moore[2]

[1]Idaho National Laboratory, Idaho Falls, ID, 83415, USA

[2]Department of Chemical Engineering, University of Utah, Salt Lake City, UT, 84112, USA Mitchell.Plummer@inl.gov

Keywords: enhanced geothermal systems, Raft River, well stimulation, cold water injection

ABSTRACT

The injection well stimulation project at the Raft River geothermal field tests the effect of long-term cold water injection and high pressure injection on well injectivity, improvements to which could reduce operating costs. The primary data for analysis and interpretation of the injection test are step-rate flow tests run before each new phase of the injection. These tests were analyzed using a combination of standard pump-test analytical solution methods and methods developed expressly for the observed conditions.

The stepped rate injection tests, combined with long-term flow and pressure response data suggest that the well is located within a fractured formation of low transmissivity but high storativity. These calculated parameters appeared to increase with pressure during the first injection test and the higher values were reproduced during the second stepped rate test. Calculated transmissivity and storativity are on the order of 4E-5 m cm^2 and 1E-4 m Pa^{-1}, respectively. The apparent pressure dependence of fitted hydraulic parameters may reflect near-well fracture compliance that increased the effective radius of the wellbore during the first test. While the type curve fit analysis also suggests that the reservoir behaves as a uniformly fractured reservoir with a radial flow regime, the hydraulic parameters indicate that condition may exist only a very limited distance (<10 m) from the well. Longer-term pressure response suggests that flow in the system effectively reaches steady state in a period of less than a day, which may reflect pressure stabilization resulting from pressure-dependent permeability or a region of much higher permeability located with a few meters of the well. The transmissivity estimates obtained from this analysis, converted to approximate fracture density and aperture, provide useful constraints on the distance to which the thermal front may migrate from the well during the cold water injection phase of the stimulation project. We estimate that the cooling front will migrate less than a tenth of a kilometer over an approximately one-year injection period. The effects of that cooling, however, may be substantial, because increases in permeability have maximum effect nearest the well.

INTRODUCTION

Whether to increase productivity of existing hydrothermal reservoirs, or to engineer new geothermal reservoirs, methods of stimulating wells to increase productivity are essential to expansion of geothermal energy. To provide a detailed study of well response to stimulation on the edges of an active hydrogeothermal system, the Department of Energy Geothermal Technology Program is sponsoring an Enhanced Geothermal System study at the Raft River Geothermal Reservoir in southern, Idaho. An existing well at that location, well RRG-9, was drilled to the depth of other productive reservoir wells but proved to have injectivity too low for economic use as either a production well or cold water injection well. The project involves application of a series of stimulation methods to well RRG-9 and detailed monitoring of the well and reservoir to better understand reservoir response to stimulation. The stimulation methods include long-term cold water injection at a variety of flow rates and injection temperatures, aimed at improving permeability by cooling and contraction of the fractured rock host formation, followed by high-pressure injections designed to alter permeability via application of fluid pressures that exceed the fracture gradient. Methods of monitoring the reservoir include high-resolution temperature logging within the well at all times, via distributed temperature sensing, seismic monitoring, periodic borehole televiewer logging, periodic stepped flow rate tests and tracer injections before and after stimulation efforts. In this paper, we discuss initial analysis of the thermal stimulation efforts in well RRG-9. Novel methods of analysis are discussed and put into perspective using numerical simulation of poroelastic behavior in the reservoir. The results should provide useful information for further analysis of thermal stimulation effects in geothermal reservoirs.

BACKGROUND

Raft River Geothermal Area

The Raft River geothermal reservoir is located in Cassia County Idaho approximately 6 miles north of the Utah/Idaho border near the town of Malta (Figure 1). This site was heavily studied by the U.S. Department of Energy from 1975 to 1982 and was the testing site of the first commercial scale binary (isobutene) cycle geothermal power plant in the world. Presently this site is owned and operated by U.S. Geothermal and is producing power from a 13-MW (nominal) binary isopentane power system.

The geologic structure in the Raft River geothermal area has been extensively studied using geophysical methods, surface mapping, aerial photography and core lithologic descriptions of subsurface core materials. The Raft River geothermal site is located near the southern end of the Raft River north-south trending valley (Figure 2). This valley is characterized by high-angle normal faulting, low-angle faulting emplacing younger over older rocks, moderate plutonism, and the presence of discontinuous metamorphic terrains (Allman et al., 1982). Beneath the surface alluvium, the Salt Lake Formation is a thick (~1200 meter) poorly consolidated deposit consisting of siltstone and sandstone. Underlying this formation is a 150 meter metamorphized unit, called the metasediments, consisting of sub-units of schist and quartzite. The base rock is a Precambrian adamellite. The western side of the valley has been down dropped along listric faults in the Bridge and Horse Well Fault zones through the Salt Lake Formation. These faults dip 60 to 80

degrees to the east at the surface and become nearly horizontal in the Tertiary Sediments and may have produced many near vertical open fractures at the base of the sediments. The Horse Well and the Bridge Faults are thought to play a significant role in the development of the Raft River geothermal reservoir (Allman et al., 1982; Dolenc et al., 1981). Movement along of these faults is believed to have created vertical fractures in the base of the Salt Lake Formation and in the underlying Precambrian metasediments that are responsible for the high well yields. A geophysical anomaly possibly representing a shear zone, called the Narrows zone, exists in the basement Precambrian.

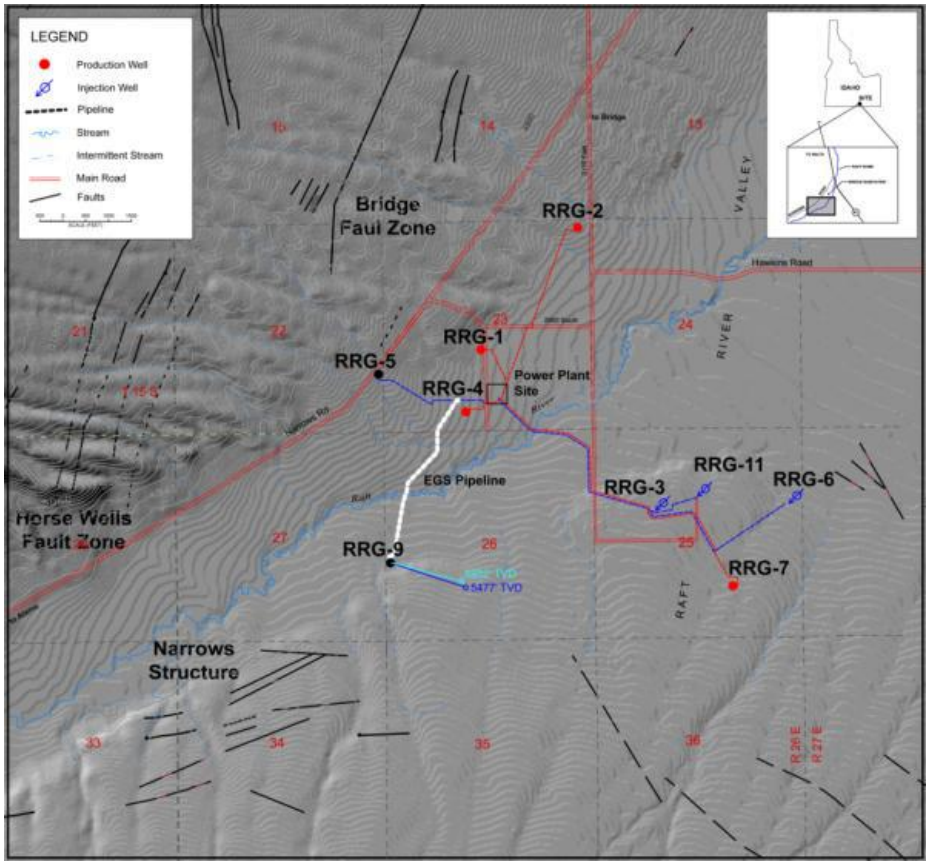

Figure 1. Map showing well locations and infrastructure within the Raft River geothermal field and major fault zones.

RRG-9 History

In this paper, we focus on the recent testing that was done in well RRG-9 which is located approximately 900 ft SSW of the power plant. Initially completed in 2007, well RRG-9 was drilled to a depth of 1856 m (6089 ft) to test reservoir properties in the intersection of the of the Narrows and Bridge Fault zones (Figure 2). The well was deviated to the east with a 44° inclination at bottom and cased to a depth of 706 m (2317 ft) MD. RRG-9 encountered the top of the Precambrian beneath the Tertiary Salt Lake Formation at 1611 m (5286 ft) MD and was completed in quartz monzonite. Due to low permeability, the well proved unproductive for energy production and as an injection well and the RRG-9 is therefore not currently used for reservoir operations. For that reason, the well is available as a stimulation target that should not interfere with reservoir operations, but other characteristics also make it a favorable location for stimulation testing. It is located relatively near the more productive fault zones, and temperature in the high permeability zone is similar to that at the primary production wells, so improvements in permeability could allow its use for either energy production or cooled water injection.

Well RRG-9 ST-1 was drilled in early 2012, during preparation for stimulation of the well. The initial efforts required drilling out a bridge plug placed near the base of the casing at 689 m (2262 ft) MD to conduct a Vertical Seismic Profiling survey. Attempts to drill through the plug failed and it was pushed down the well to about 1372 m (4500 ft) MD, at which point the bit deviated from the original borehole. The sidetrack hole, RRG-9 ST-1, was drilled to a TD of 1808 m (5932 ft) MD, in the Lower Narrows Schist, and cased to 1692 m (5551 ft) MD.

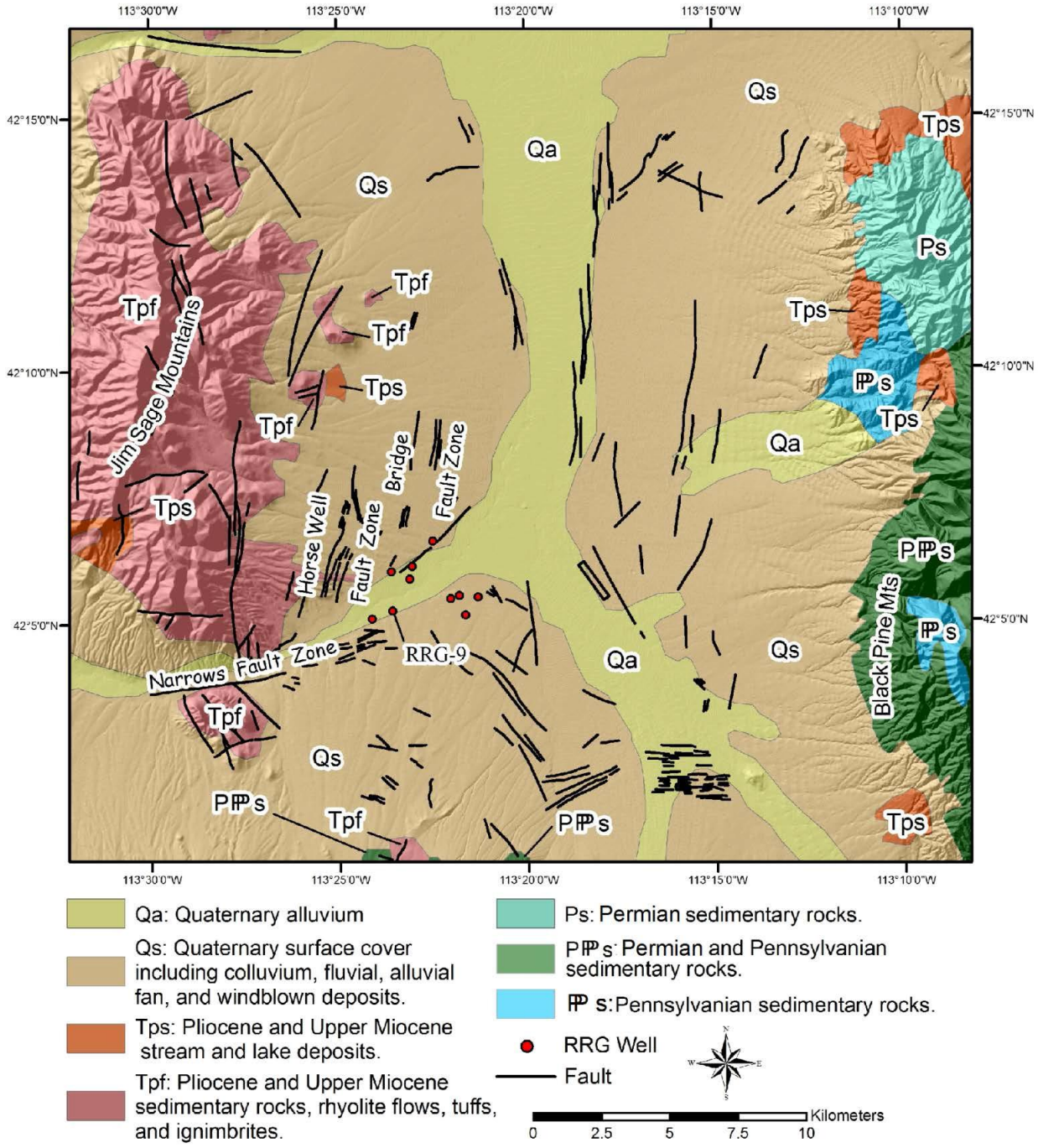

Figure 2. Geologic map of the Raft River geothermal area (Williams and others, 1974). RRG-9 is the site of the target well. Red dots show other deep geothermal wells. The major production wells are located to the north of RRG-9, in the Bridge Fault Zone. The Narrows Fault Zone is believed to separate RRG-9 from the productive Bridge Fault Zone.

Well Stimulation

A multi-phase stimulation program is in progress at well RRG-9 ST-1 (Table 1). Phase I of the stimulation began on June 13, 2013 with injection from the power plant at a temperature of about 39 °C, pressure of 275 psig and flow rate of approximately 40 gpm. That injection continued until August 20, 2013, and was immediately followed by a stepped rate injection test, on August 22, 2013, prior to initiation of the next phase of injection. That test was aimed at detecting differences in reservoir behavior as compared to a similar, February 24, 2012 test conducted well before Phase I of the stimulation. In phase II, two positive displacement plunger type pumps were used to increase the injection pressure and flow rate for about one month. The highest rate achieved was 261 gpm at a pressure of 809 psig. During this time, fluid from the cooler water well was injected for about two weeks at various pressures. Then, the pumps were

removed and plant injection resumed on 25 September, 2013. Flow rates and wellhead pressures between resumption of plant water injection have been approximately 122-133 gpm at 272-281 psi. This injection phase will continue until the spring of 2014, when a high pressure hydraulic stimulation will be conducted.

Table 1. Injection history during the cold-water injection stimulation phases at well RRG-9.

Source	Booster Pump(s)	Time Period	Flow Rate (gpm)	Average WHP (psi)	Average Fluid Temperature (°C)
Plant Injectate	No	13-Jun to 20-Aug	43	280	39
Plant Injectate	No	23-Aug to 30-Aug	141	540	40
Plant Injectate	Yes	1-Sep to 8-Sep	261	809	46
Cold Well Water	Yes	12-Sep to 16-Sep	254	743	12
Cold Well Water	Yes	16-Sep to 24-Sep	191	522	13
Plant Injectate	No	25-Sep to 2-Dec	122	272	30
Plant Injectate	No	3-Dec to 15-Feb	133	281	27

Stepped Rate Injection Testing

Primary information about the response of the reservoir to stimulation activities comes from the pressure – flow relationship measured during periodic stepped rate injection tests, which describe pressure change in the well to constant injection rates designed to produce a range of injection pressure. In this report, we summarize analyses of the injection tests using standard type curve methods aimed at characterizing the primary hydraulic properties of the reservoir. This paper thus focuses on analysis of transient pressure data. See Bradford et al. (2014) for a discussion of apparent steady-state injection behavior and trends during the cold-water injection phase of the stimulation tests.

February 24, 2012 Step Rate Test

On February 24, 2012 a stepped injection rate test was performed on the open-hole segment of RRG-9 ST-1. Water was pumped at rates of 13 to 788 gpm with each step lasting approximately 15-30 minutes. The maximum wellhead pressure attained was approximately 1150 psig. Injection rates were then reduced from 630 to 11 gpm. A total of 81,648 gal was injected. Figure 3A shows well pressure and injection rate information from the first five steps of that test.

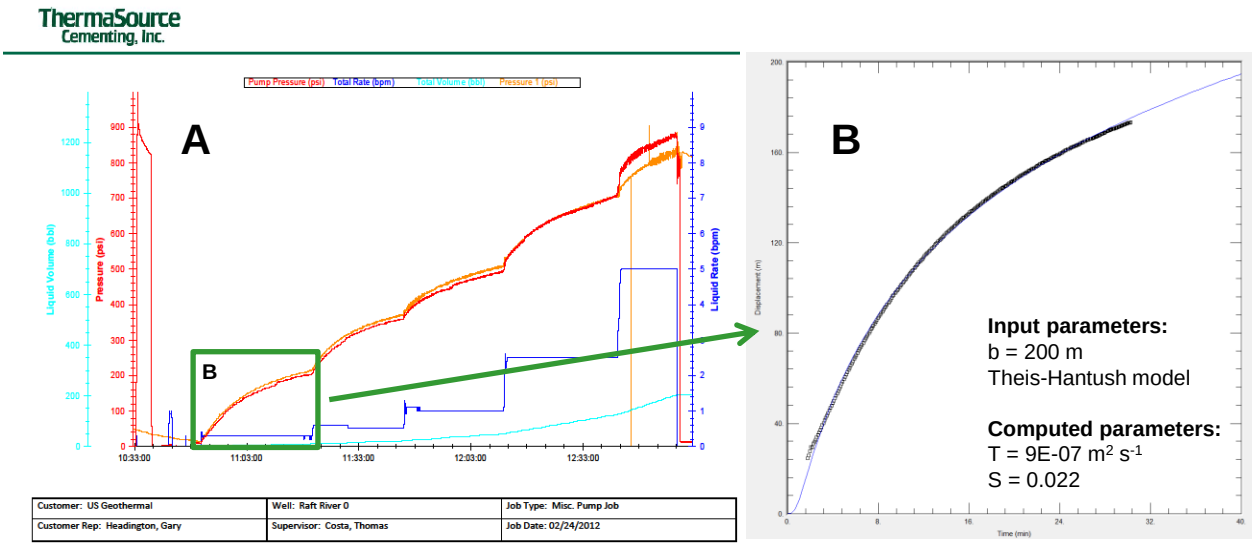

Figure 3. (A) February 24, 2012 step rate test conditions from 10:33 to 13:00. The dark blue and light blue lines represent the liquid pumping rate and cumulative volume respectively. The red and orange lines are the measured pressure. (B) Best-fit Theis-Hantush curve solution and parameters from analysis using Aqtesolv, from first step of data in A.

August 22, 2013 Step Rate Test

Following the initial phase of cold water injection, a second stepped injection rate test was conducted on August 24, 2013. Based on analysis of the earlier stepped rate test, injection step duration was increased during this test, to attempt to capture more of the transient pressure response. Flow rates varied between approximately 65 and 340 gpm, in a sequence of seven steps lasting from 36 to 129 minutes, with the last change occurring 540 minutes after the start of the test (Figure 4B). The maximum wellhead pressure attained was approximately 930 psig.

RESULTS AND DISCUSSION

Initial Reservoir Properties

The step-rate tests provide a means of determining the overall permeability and storativity of the reservoir connected to well RRG-9, and how the system responds to increasing and decreasing injection pressure. This information is critical for estimating how the cooling front induced by cold water injection will propagate through the reservoir and for understanding how cold-water stimulation and high-pressure injection stimulation efforts may affect the well's injectivity. Because the flow rates and pressures in the first step of the February step-rate test were the lowest (Figure 4), we used the data from that step to determine the initial hydrologic parameters for the reservoir. We used the commercial package Aqtesolv (Duffield, 2007) to test a variety of reservoir response models, including, for example, models incorporating vertical and horizontal fractures, aquifers with leakage from surrounding formations, partial penetrating wells and wellbore storage. Results demonstrated that the Theis-Hantush type curve, or similar models assuming essentially uniform radial flow, provided substantially better fit than more heterogeneous models. Our estimates of transmissivity and storativity for the fracture network, and further analyses of response during stepped changes in flow rate are, therefore, based on the Theis-Hantush model of well response to pumping. Transmissivity (the product of the intrinsic permeability (k) and reservoir thickness (b)) estimated from the curve-fitting process is 2E-10 cm^3 (or 9.4E-7 m^2 s^{-1}, in hydraulic head– based units). Assuming a fractured zone thickness of between 10 and 100 m for the target zone, the Elba Quartzite, this suggests a bulk intrinsic permeability of 2E-11 cm^2 to 2E-12 cm^2, at the low end of the range commonly estimated for fractured igneous and metamorphic rock (~1E-11 cm^2 – 1E-7 cm^2, Freeze and Cherry, 1979). While the relatively low transmissivity is consistent with the historically poor injectivity of well RRG-9, the storativity determined from the analysis, 2.6E-6 m Pa^{-1} (~0.026 in hydraulic head- based units) is large. Again assuming a fracture zone thickness of between 10 and 100 m, this implies a bulk rock compressibility (neglecting the much smaller compressibility of water) of between 2E-8 Pa^{-1} and 2E-7 Pa^{-1}. Only the lowest value in that range, which assumes a fractured zone thickness of 100 m, overlaps with the range suggested by Freeze and Cherry (1979) for jointed rock compressibility, 1E-10 Pa^{-1} to 1E-8 Pa^{-1}.

The relatively large compressibility calculated from type curve analysis, and relatively low transmissivity suggest that other effects that can produce that behavior must be carefully examined. Wellbore storage effects, for example, can be incorrectly interpreted as high storativity and inclusion of wellbore storage effects in the first step of the first step-rate test does substantially improve the quality of the fit, but only with a casing radius that provides approximately 8% of the volume per unit height of the actual well casing. Moreover, water flow into the sealed pump-wellhead system at RRG-9 is such that early-time changes in water level would compress the initial gas volume under static water conditions, creating a non-linear wellbore storage effect that would diminish rapidly. Early time data considered in the first and second tests begins at approximately 150 psi and 270 psi, respectively. Based on in-hole pressure and temperature data obtained prior to the test, the static water level at atmospheric pressure was approximately 55 m below ground surface. Thus, at the starting gage pressures, Δp, considered during our analyses, the water level rise above the static condition ΔH, is given by

$$\Delta H = s_{initial} * \frac{\Delta p}{p_{atm} + \Delta p}$$

where p_{atm} is atmospheric pressure and $s_{initial}$ is the initial depth of water below the wellhead, and the resulting values are 52 and 54 m, respectively, demonstrating that little pressurized gas space remains to accommodate wellbore storage. Compression of water in the ~6089 ft wellbore can also be shown to provide an insignificant wellbore storage component, and we conclude that wellbore storage effects can safely be neglected. A remaining complication for both step-rate tests is that unsteady flow rates during preparation for the tests in both cases established a slightly decreasing pressure transient. Superposition of that poorly defined pressure decay on the step test data could explain some part of the apparent storativity values for the initial steps in both tests.

The relatively low permeability but high storativity calculated for the fractured system provide somewhat conflicting information about the effective thickness of the fracture network accessed by well RRG-9; low transmissivity suggests relatively low thickness while high storativity suggests the opposite. Additional information for estimating that thickness is derived from the several different methods of borehole logging applied in this project. Borehole televiewer data and well logs indicate that within the Elba Quartzite, the RRG-9 intersects several large open fractures at approximately 1722 m (5650 ft) and that static borehole temperature is reduced in that region. Approximately 76 fractures were mapped between 1704 m (5592 ft) and 1789 m (5870 ft) in the Elba Quartzite, suggesting an average fracture density of 0.9 m^{-1} and additional fractures were identified in the underlying Lower Narrows Schist. The thickness of the Elba Quartzite at RRG-9 is approximately 175 m. If we assume similar fracture density throughout, then the implied specific storage of the formation is about 1.5E-8 Pa-1, at the upper end of suggested values for fractured rock according to several sources (Freeze and Cherry, 1979; Domenico, and Mifflin, 1965; Singhal and Gupta, 2010).

Combined with the transmissivity estimate from the type-curve analysis, we conclude that the fracture network of the Elba Quartzite consists of relatively low-permeability fractures but with relatively large bulk compressibility. Assuming that transmissivity is related to aperture by the cubic law, (Domenico and Schwartz, 1990),

$$b = \left(\frac{12Tr}{N_f} \right)^{1/3}$$

we can estimate the effective aperture, *b*, of one or more such fractures from the transmissivity, *Tr*, and the assumed number of fractures, *Nf*, providing flow in a hypothetical radial flow system of parallel fractures. While this approach vastly oversimplifies the distribution of any real fracture network, the resulting fracture apertures and spacing are useful reference points for constraining the behavior of the system. Taking the number of fractures as between a minimum of one and a maximum value derived from the fracture density estimated for the Elba Quartzite, a single fracture with an effective aperture of 0.06 mm or a network of ~160 fractures of 0.011 mm could provide the transmissivity estimated for well RRG-9.

Stepped Injection Rate Test Analysis

Where hydrogeologic properties are constant, the stepped injection rate test is commonly used to infer changes in well efficiency or other hydraulic properties. Our analysis of the RRG-9 tests, however, indicates that standard well efficiency equations do not provide a good fit to the changes in pressure induced by the changes in flow rate. None of the step-drawdown methods available in the Aqtesolv package, for example, provided a reasonable fit to the data. Hypothesizing that transmissivity and storativity may be locally altered by increasing fluid pressure, we developed a superposition algorithm, using PTC's Mathcad software, that performs non-linear least squares regression to fit the stepped injection rate test data by allowing both those parameters to vary between steps. Results yielded a good fit to both the February 2012 and August 2013 step tests (Figure 4), with significantly varying transmissivity and storativity between both within and between the tests (Figure 5). The fit is markedly better than if transmissivity and storativity are assumed to remain fixed (Figure 4A).

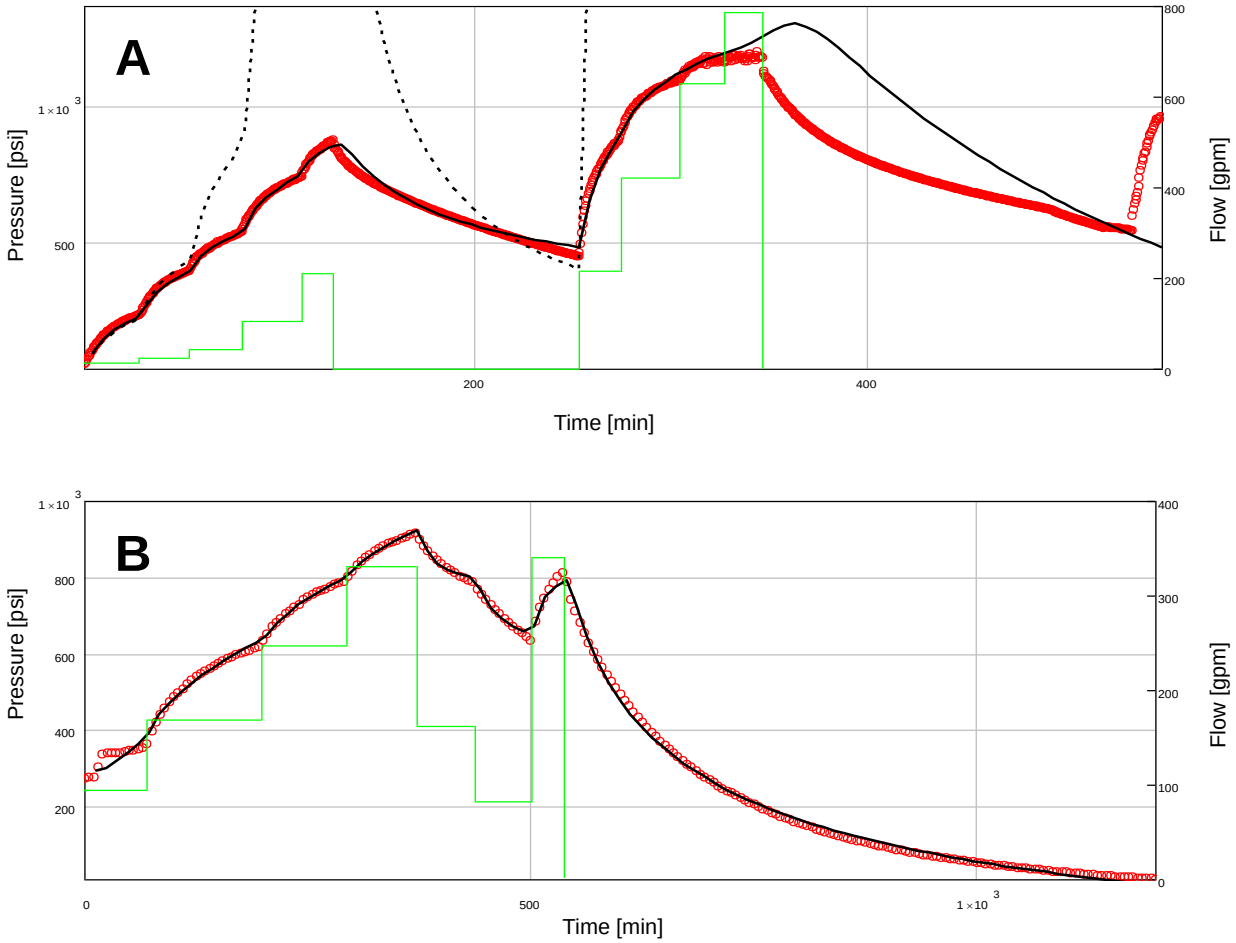

Figure 4. Superposition solution for the (A) February 2012 and (B) August 2013 step drawdown tests. Red symbols show measured wellhead pressures and dashed black line shows best-fit Theis-Hantush solution curve, assuming variable transmissivity and storativity. Green line describes flow rates during the tests. Note that data timing issues unresolved at the time of this submission prevented analysis of data in the Feb 2012 test after approximately 500 min. Black dashed line in upper graph (A) shows Theis curve for the stepped rate test assuming constant transmissivity and storativity equal to that determined for the first step.

Plotted against the mean pressure during each step, the apparent increases in transmissivity during the February 2012 test were non-linearly related to pressure increase, with an approximately 5-fold increase in injection pressure producing almost two orders of magnitude increase in transmissivity. Apparent transmissivities also increased dramatically at an injection pressure of approximately 800 psi. Apparent storativities also appeared to display a log-linear relationship with injection pressure. The highest calculated value of that parameter was almost three orders of magnitude greater than that determined from the lowest injection pressures, but even discounting that value as an outlier, the bulk of the data indicate suggest that a doubling of fluid pressure yields more than a 3-fold increase in storativity . These results, measured before the beginning of the cold water injection phase of the stimulation, suggest a strong poroelastic response in the system. Expansion of the fractured rock matrix would, however, likely reduce storativity as pressure increases, as resistance of the surrounding rock would increase as the fracture matrix expands against it. As an an alternative explanation for the apparent increases in storativity, consider that in the Theis equation for drawdown, $s = \frac{Q}{4\pi T} W(u)$, u is a function of well radius, storativity, transmissivity and time, $u = \frac{r^2 S}{4Tt}$, and that the well radius appears only with the storativity term. For that reason, effective well radius is sometimes included as a term in the well function argument, u, though generally as a reduction in radius due to well screen skin effects. At RRG-9, we hypothesize that the effective well radius is increased during the step test due to the compliance of the fractures transmitting flow. The effective well radius in this case represents the maximum radial position near the well at which pressure gradients are effectively negligible compared to that in larger formation. This effective radius is related to the actual radius by

$$r_w{}^2 S = r_e{}^2 S_{actual}$$

where r_w is the actual well radius, S, the curve-fit specific storage, r_e , the effective well radius, and S_{actual} is the actual rock compressibility. This relationship indicates that apparent specific storage should increase as the square of the effective well radius, so apparent increases of one to two orders of magnitude in storativity test could represent three- to ten-fold increases in effective well radius. Starting with an initial effective aperture equal to the well radius, this would imply significant fracture expansion to a radius of

~0.4 to 1 meters. Because permeability increases as the cube of fracture aperture, small increases in aperture may readily reduce local pressure gradients to the point where the effective well radius is substantially increased. The mechanism for such a change is, however, a function of fracture compliance, which depends on the stress carried by asperities, fluid pressure and mechanical strength of the surrounding rock. Work is currently underway at INL to fit these step test data using a physical model of fracture compliance similar to that described by Svenson et al. (2007), to determine whether these apparent changes in storativity can be reproduced using physically based estimates of fracture response to increased fluid pressure.

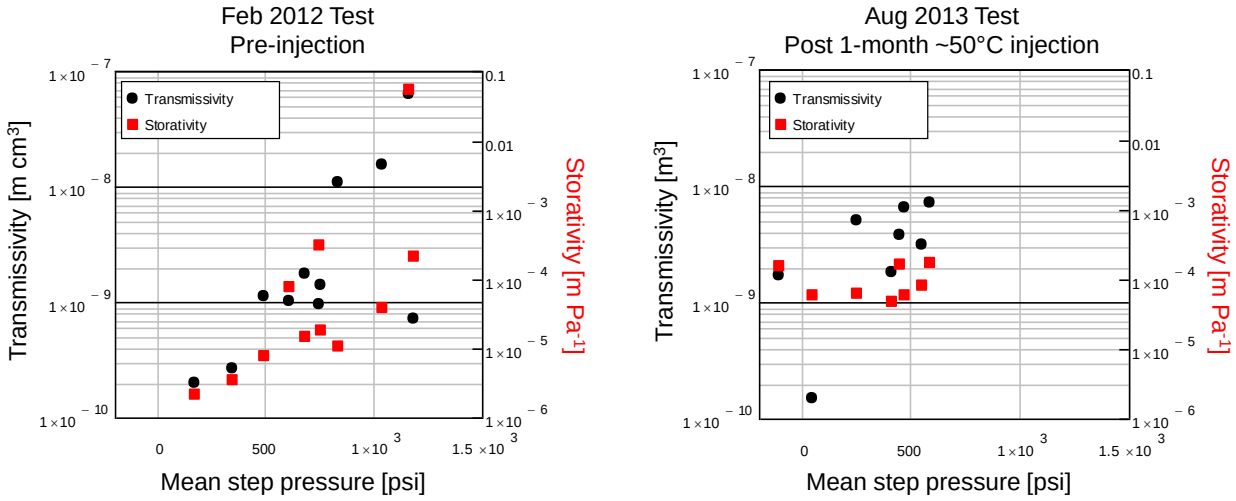

Figure 5. Best-fit aquifer properties for the data shown in Figure 4.

Apparent changes in transmissivity and storativity as a function of pressure during the second stepped rate test were markedly diminished compared to those observed in the February test. While calculated transmissivity values varied considerably, storativity appeared effectively constant. The most striking difference between the two tests, however, is that at similar pressures transmissivity and storativity in the second test appear to be generally higher than in the first test, particularly at the lower pressures induced by lower injection rates. Because the second test occurred after several months of cold water injection, it is possible that these increases represent cooling-induced dilation of fractures, whether via shearing or expansion. These analyses do not include the latest time data of the first stepped rate test, which would help to determine whether the increases in transmissivity and storativity observed during that test were transient or semi-permanent.

According to the radial flow model implied by the above analysis, pressure would continue to increase during constant injection, but at a rate that diminishes with time. This is contrary, however, to what is observed in the long-term pressure response. Figure 6 illustrates well response during a 12-day period in early September, during which the flow rate changed dramatically on several occasions, and which evidences long-term pressure response to initially steady pressure. At 3.5 days in this record, the well returns to steady injection after a period of greatly reduced injection rate, and at 8 days in, the well recovers to zero gage pressure after a long period of steady flow and pressure. In each case, the pressure appears to reach steady state in approximately 18 hours. This suggests that a modified Hall plot analysis of the long-term flow and pressure data may provide a good measure of permeability and changes in permeability over time, because the radius of influence of the well may be effectively constant after only a short period of steady injection. See Bradford et al. (these proceedings) for that analysis.

We suggest two possible explanations for the relatively rapid approach to equilibrium fluid pressure. The first involves pressure-dependent permeability associated with fracture compliance. In this scenario, increasing permeability resulting from the expanding zone of higher fluid pressure compensates for the increasing pressure to maintain equilibrium at a lower maximum pressure. While we have demonstrated that pressure dependent permeability can produce an apparent steady state over relatively short timescales, we have yet to reproduce such behavior using realistic physically based models of fracture mechanics. A second possible explanation is that the pressure gradient distal to the well reaches, within one day, a region of significantly higher permeability that effectively behaves as a constant flow boundary to the well. The transmissivity and high storativity implied by the transient stepped rate tests provide some constraint on the distance to that hypothetical boundary. Based on those properties, the effective radius of influence of the injection (ie. the radial distance at which pressure has returned to ambient reservoir pressure), after one day, would be approximately 6 m. Applying a bounded solution to the Theis type curve for the pressure decline observed at the 8-day mark in Figure 6 indicates that a reasonable fit to the curve can be obtained with constant head boundaries approximately 0.5 m from the well.

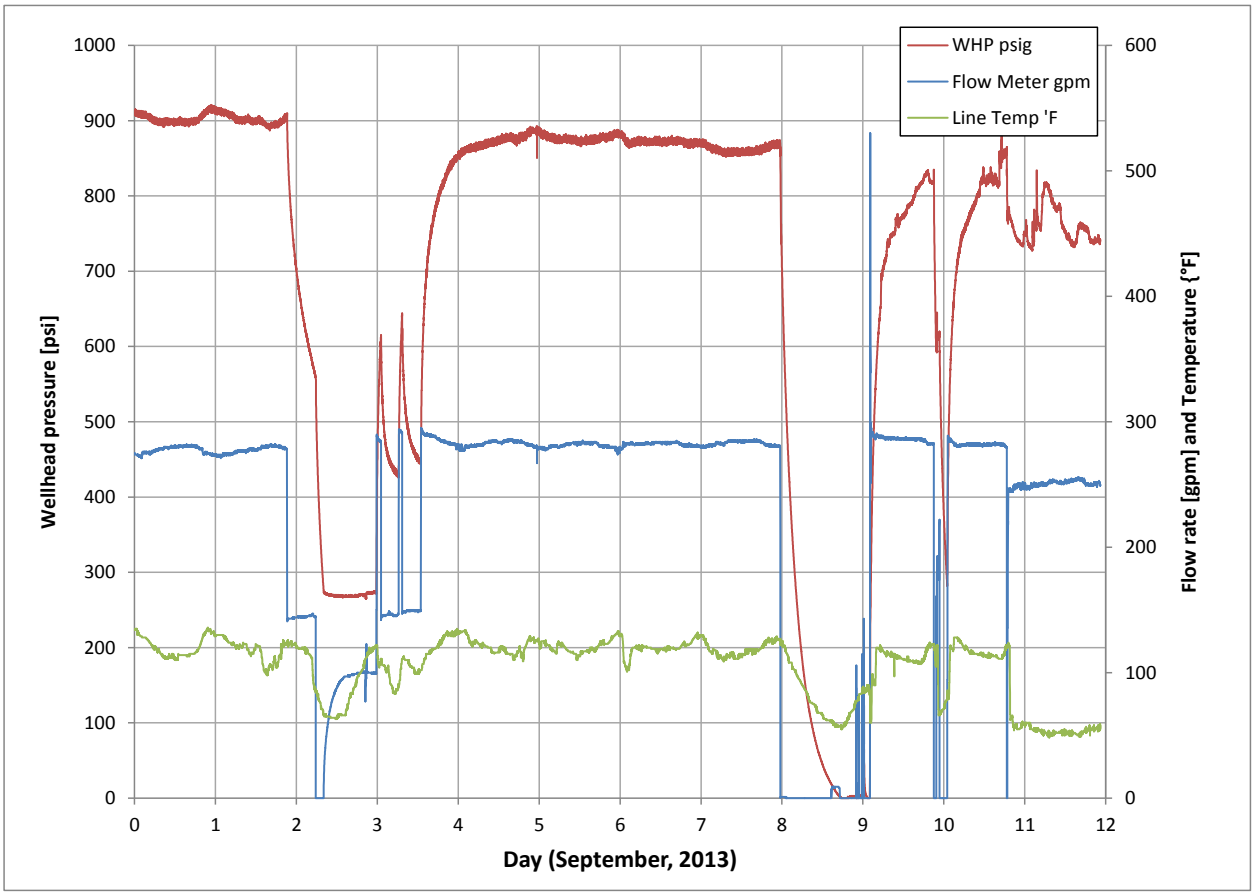

Figure 6. Wellhead pressure, injection rate, and injection line temperature during a 12-day period in early September, 2013, evidencing long-term pressure response during two ~1-day periods following a large change in flow rate.

Cooling Effects implied from Step-Rate Tests

Depending on its mechanical response to cooling, the effect of cold water injection on the formation may include dilation, shearing or extension of existing fractures. Consequent improvement in injectivity may result from one of two mechanisms. The first of these involves improving or creating permeability along pathways that intersect more productive, higher permeability, regions of the system. The probability of producing such distal effects can be expected to increase as the cooling front migrates outward from the well, as the number of intersected fractures increases. The second is near-well enhancement of permeability that consequently reduces pressure gradients near the well, where pressure gradients are greatest. Thus proximal cooling can improve well productivity even if no distal connections to regions of higher permeability are made.

Because the probability of producing connections to zones of greater permeability increases as the cooled region expands, it is useful to estimate the likely behavior of the cooling front during the stimulation. As a first-order estimate of how the cooling front might progress, we use commonly applied analytical solutions for heat transport in fractured rock of relatively simple geometry. Based on flow data that suggests that steady state pressures are achieved at well RRG-9 after 18 hours, we assume a steady state flow regime. We neglect the several changes in flow rates and temperatures induced during various stimulation phases at RRG-9 and consider only the long term flow rate and relative temperature change, where relative temperature is defined as

$$T_{rel} = \frac{T - T_{inj}}{T_{res} - T_{inj}}$$

and T is temperature, T_{inj} is the injection temperature and T_{res} the background reservoir temperature. For injection, we assume a flow rate of 120 gpm in a fractured zone with a maximum thickness of 200 m, and assume that injection occurs for a maximum period of one year. Fluid and rock characteristics are as summarized in Appendix A.

Based on the stepped injection rate test data, the fracture network connected to RRG-9 appears to behave as a relatively homogeneous isotropic permeable unit, representative, perhaps, of one or more areally extensive subhorizontal fractures. As previously mentioned, the apparent transmissivity of the formation appears to be readily accommodated by a single fracture with an effective aperture of 0.06 mm. Because the distance to which the cooling front would propagate is inversely related to the number of fractures through which flow occurs, we consider the flow and heat transport behavior in a single fracture as a useful measure of the upper limit of that migration rate.

This assumption also explores a possibility suggested by some of the available borehole data; high-resolution temperature monitoring of the well during cold water injection suggests that most of the injected water enters the formation over an interval between 1719 m (5640 ft) and 1725 m (5660 ft), and a large fracture appears in the televiewer logs at that depth.

In the proposed flow scenario, cooling of the fracture can be calculated using an analytical solution of the advection dispersion equation for radial flow (Figure 7) (Feenstra et al. 1984). For the single-fracture radial flow scenario, the cooling front, here defined as the position at which the relative temperature equals 0.5, reaches approximately 70 m after one year, while the leading edge of the cooling front reaches a distance of approximately 130 m (Figure 8A). In addition, because both the radial flow regime and the thermal response essentially proceed as the square root of time, the migration of the cooling front is proportional to $t^{¼}$ (Figure 9). For comparison, if the same flow is injected into the middle of an infinitely long, 100-m high, fracture of the same aperture, the cooling front migrates (Carslaw and Jaeger, 1959) significantly faster, reaching approximately 100 m at one year, with propagation proportional $\sqrt{t}$. In the linear flow case, however, the front is also much more diffuse (Figure 8B), so that the leading edge of the cooling front migrates much faster than in the radial flow case.

These single-fracture scenarios provide some insight into the likely extent of cooling induced by long-term cold water injection at RRG-9, because the transmissivity may be dominated by a limited number of larger fractures. While non-uniform fracture aperture distribution in such a system could cause even more extensive radial propagation of the cooling front, flow from RRG-9 - in reality - is likely conducted by a more complicated fracture pattern, for which more of the cooling effects would occur proximal to the well. When the injection flow is divided among many fractures, propagation rate is inversely proportional to the number of fractures and is, again, retarded relative to the fluid injection front. Using the average fracture density of the section of Elba Quartzite seen in the borehole televiewer data (~0.9 fractures per meter), the thermal front would lag the fluid front by a factor of approximately 7E4. Thus, the cooling front in a 1D flow system as described above, with the same flow conducted equally by ~160 fractures would migrate only a distance of approximately 10 meters from the source, relative to the fluid front which would theoretically reach a distance of 700 km in the same 1-year period.

These calculations suggest that the cooling front for a one-year cold water injection is unlikely to migrate much further than about a tenth of a kilometer. For comparison, the distance to the closest well (RRG-4) located in the productive portion of the reservoir is 1.3 km (0.8 miles). If the width of the Narrows Fault Zone separating RRG-9 from the more productive fault zones is on the order of a kilometer, then cooling-induced improvements in hydraulic communication with the latter are likely to occur only if high-permeability fractures already extend across the former. The dilation of fractures around the well, however, can substantially reduce pressure gradients around the well, where pressure gradients are greatest. Available data from the stepped rate injection tests suggests that such effects may have occurred as soon as three months after the onset of cold water injection.

CONCLUSIONS

The stepped rate injection tests completed during the cold water injection stimulation phase at RRG-9, combined with long-term flow and pressure response data suggest that the open section of the well is located within a fractured formation of low transmissivity but high

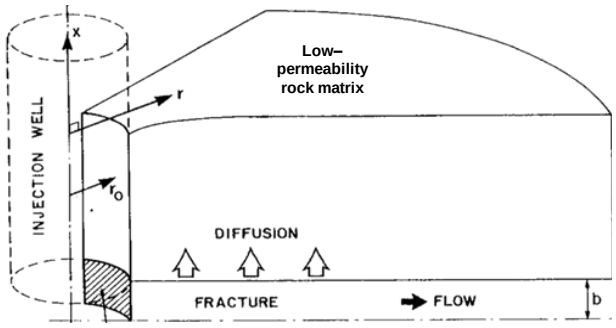

Figure 7. Schematic illustrating the geometry of the radial flow into a set of parallel, uniformly spaced, horizontal infinite fractures, from Feenstra et al. (1984).

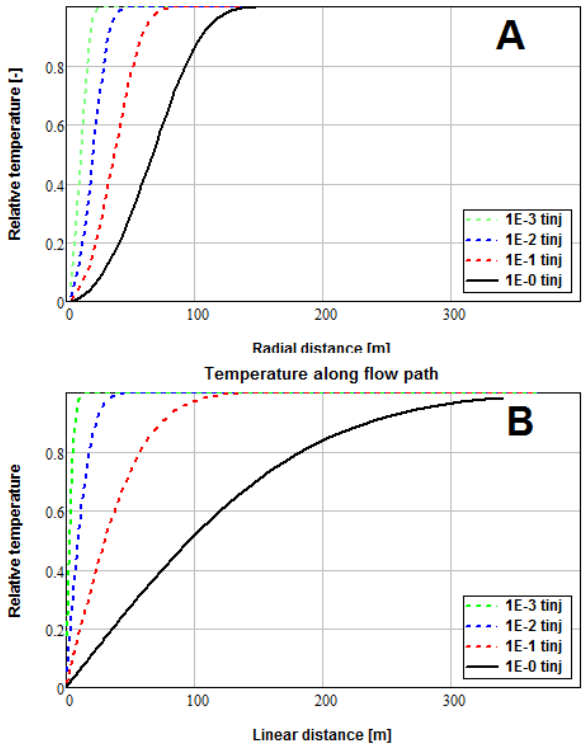

Figure 8. Plots illustrating response of a hypothetical fracture system to a one-year cold water injection period, for a (A) radial flow system and (B) a linear flow system.

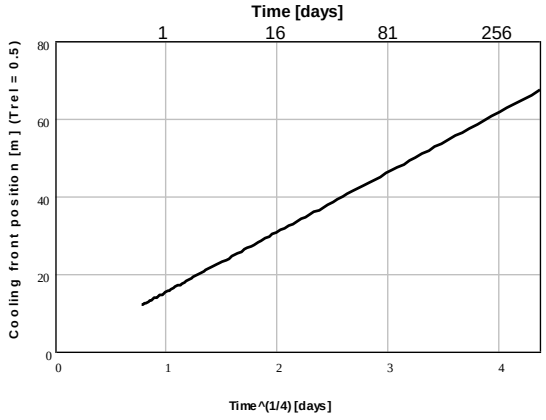

Figure 9. Cooling front (where T_{rel} = 0.5) position vs time in a radial flow system, illustrating linear relationship with $t^{¼}$.

storativity. Calculated values for those parameters appeared to increase with pressure during the first injection test and the higher values were reproduced during the second stepped rate test. Based on the latter data, the apparent transmissivity and storativity are on the order of 4E-5 m cm^2 and 1E-4 m Pa^{-1}. Based on our type-curve analysis of the data, we conclude that the apparent pressure dependence of fitted hydraulic parameters reflects near-well fracture compliance that increased the effective radius of the wellbore during the first test. While the type curve fit analysis also suggests that the reservoir behaves as a uniformly fractured reservoir, with a radial flow regime, the hydraulic parameters indicate that that condition may exist over only a limited radial distance (<10 m) from the well. Longer-term pressure response suggests that flow in the system effectively reaches steady state in a period of less than a day, which may reflect pressure stabilization resulting from pressure-dependent permeability or a region of much higher permeability located with a few meters of the well.

The transmissivity estimates obtained from this analysis, converted to approximate fracture density and aperture, provide useful constraints on the distance to which the thermal front may migrate from the well during the cold water injection phase of the stimulation project. While the propagation rates depends on a number of factors, including the large-scale flow regime and fracture distribution, that are difficult to determine, we estimate that the cooling front will migrate less than a tenth of a kilometer over an approximately one-year injection period. The effects of that cooling, however, may be substantial, because increases in permeability have maximum effect nearest the well.

REFERENCES

Allman, D.W., Tullis, J.A, Dolenc, M.R., Thurow, T.L. and Skiba P.A. (1982), "Raft River Monitor Well Potentiometric Head Responses and Water Quality as Related to the Conceptual Ground-Water Flow System", EG&G Idaho Inc. Technical Report (EGG-2215), Vol. II, prepared for the US Department of Energy, Idaho Operations Office.

Bradford, J., J. McLennan, J. Moore, D. Glaspey, D. Waters, R. Kruwell, A. Bailey, W. Rickard, K. Bloomfield, and D.King, Recent Developments at the Raft River Geothermal Field, Proceedings, Thirty-Eighth Workshop on Geothermal Reservoir Engineering, Stanford University, Stanford, California, February 11-13, 2013.

Bradford, J., M. Ohren, W. Osborn, J. McLennan, J. Moore, and R. Podgorney, Thermal Stimulation and Injectivity Testing at Raft River, ID EGS Site, Proceedings, Thirty-Ninth Workshop on Geothermal Reservoir Engineering, Stanford University, Stanford, California, February 24-26, 2014.

Carslaw, H.S., and J.C. Jaeger (1959), *Conduction of Heat in Solids*. Oxford University Press, Oxford, U.K., 510 p.

Dolenc, M.R., Hull, L.C., Mizell, S.A., Russell, B.F., Skiba, P.A., Strawn, J.A., and Tullis J.A. (1981), "River River Geoscience Case Study", EG&G Idaho Inc. Technical Report (EGG-2125), Vol. I, prepared for the US Department of Energy, Idaho Operations Office

Domenico, P .A. and M. D. Mifflin (1965): Water from Low-Permeability Sediments and Land Subsidence; Water Resources Research, Volume 1, Number 4, pages 563-567.

Domenico, P.A. and F.W. Schwartz (1990) Physical and Chemical Hydrogeology, John Wiley and Sons, Section 3.4, p. 87.

Duffield, G.M., 2007. AQTESOLV for Windows Version 4.5 User's Guide, HydroSOLVE, Inc., Reston, VA.

Enhanced Geothermal Systems – Concept Testing and Development at the Raft River Geothermal Field, Idaho, Stage Gate Report submitted by Energy & Geoscience Institute at the University of Utah, August 2012

Feenstra, S., J. Cherry, E. Sudicky and Zia Haq (1984) Matrix diffusion effects on contaminant migration from an injection well in fractured sandstone, Groundwater, Vol. 22, No. 3, pp. 307-316.

Freeze, R.A. and J.A. Cherry, 1979. Groundwater, Prentice Hall, Englewood Cliffs, New Jersey, 604p.

Gringarten, A.C., P.A. Witherspoon, and Y. Ohnishi (1975), "Theory of heat extraction from fractured hot dry rock." Journal of Geophysical Research. Vol. 80 , No.8, pp. 1120-1124.

National Academy, 1996. Rock Fractures and Fluid Flow - Contemporary Understanding and Applications. Committee on Fracture Characterization and Fluid Flow, National Academy Press, Washington, 551 pp.

Singhal, B.B.S and R.P. Gupta, 2010, Applied Hydrogeology of Fractured Rocks: Second Edition, Springer, New York, 428 pages.

Svenson, E., T. Schweisinger, L. Murdoch (2007) Analysis of the hydromechanical behavior of a flat-lying fracture during a slug test, Journal of Hydrology, Vol. 347, 35-47.

Williams, P. L., K, L, Pierce, D, H, McIntire, and P. W. Schmidt, 1974. Preliminary geologic map of the southern Raft River area, U.S.G.S. Open File Report, 1:24,000.

APPENDIX A

Fluid and rock characteristics

Thermal conductivity, rock $\lambda_r := 6 \cdot W \cdot m^{-1} \cdot K^{-1}$

Thermal conductivity, fluid $\lambda_f := 0.8 \cdot W \cdot m^{-1} \cdot K^{-1}$

Density, rock $\rho_r := 2650 \cdot kg \cdot m^{-3}$

Density, fluid $\rho_f := \rho_w(140) = 925.084 \frac{kg}{m^3}$

Specific heat, rock $c_r := 1050 \cdot J \cdot kg^{-1} \cdot K^{-1} = 0.251 \cdot \frac{cal}{K \cdot gm}$

Specific heat, fluid $c_f := 4186 \cdot J \cdot kg^{-1} \cdot K^{-1} = 1 \cdot \frac{cal}{K \cdot gm}$

Volumetric heat capacity, rock $C_f := \rho_f \cdot c_f = 3.872 \times 10^6 \cdot J \cdot m^{-3} \cdot K^{-1}$

Volumetric heat capacity, fluid $C_r := \rho_r \cdot c_r = 2.783 \times 10^6 \cdot J \cdot m^{-3} \cdot K^{-1}$

Thermal diffusivity, rock $\alpha_r := \frac{\lambda_r}{c_r \cdot \rho_r} = 2.156 \times 10^{-6} \frac{m^2}{s}$

Dynamic viscosity, fluid $\mu_f := 0.282 \cdot 10^{-3} \cdot \frac{N \cdot s}{m^2} = 5.89 \times 10^{-6} s \cdot \frac{lbf}{ft^2}$

Coefficient of thermal expansion